

Radiative and non-radiative recombination in CuInS₂ nanocrystals and CuInS₂-based core/shell nanocrystals

Anne C. Berends[‡], Freddy T. Rabouw^{‡§}, Frank C.M. Spoor[†], Eva Bladt[#], Sara Bals[#], Arjan J. Houtepen[†], Laurens D.A. Siebbeles[†], Celso de Mello Donegá^{‡}*

[‡] Condensed Matter and Interfaces, Debye Institute for Nanomaterials Science, Utrecht University, P.O. Box 80 000, 3508 TA Utrecht, The Netherlands.

[†] Optoelectronic Materials Section, Department of Chemical Engineering, Delft University of Technology, Van der Maasweg 9, 2629 HZ Delft, The Netherlands

[#] Electron Microscopy for Materials Science (EMAT), University of Antwerp, Groenenborgerlaan 171, B-2020 Antwerp, Belgium

ABSTRACT. Luminescent copper indium sulfide (CIS) nanocrystals (NCs) are a potential solution to the toxicity issues associated with Cd- and Pb-based nanocrystals. However, the origin of the photoluminescence (PL) and the quantum yield (QY) limiting processes in CIS NCs are still subject of a lively scientific debate. Here we provide insight in the different exciton decay pathways in CIS NCs using time-resolved PL and transient absorption (TA) spectroscopy. CIS core NCs, CIS/ZnS core/shell NCs and CIS/CdS core/shell NCs were studied to obtain information for NCs with a low PL QY (2%, core NCs) as well as a high PL QY (86%, CIS/CdS core/shell NCs), on both ps-ns timescales (TA spectroscopy) as well as ns- μ s timescales (PL spectroscopy). Quantitative analysis of the TA signals shows initially uncoupled pathways for the electron and the hole in NCs with a low PL QY, until the exciton eventually recombines. Our study indicates that the PL in CIS and CIS-based core/shell NCs originates from recombination of a quantized conduction band electron state with a localized hole. Moreover, our results show that the decay pathway of the electron determines whether the exciton recombines radiatively or non-radiatively. This is an important key in the development of high PL QY CIS-based NCs for applications.

KEYWORDS: nanocrystals, copper indium sulfide, exciton dynamics, transient absorption spectroscopy.

Semiconductor nanocrystals (NCs) show intriguing optoelectronic properties that differ from bulk and depend on the size and shape of the nanocrystal.¹ These new properties make semiconductor NCs interesting materials for a number of applications, such as batteries, electronics, light emitting diodes, lasers, photodetectors, solar cells and theranostics.² Cadmium and lead chalcogenide NCs are the most extensively studied photoluminescent semiconductor NCs, showing emission in the visible and near infrared spectral window. However, their utilization in consumer products is limited by toxicity concerns. This has motivated an increasing research effort on compositions that are based on less toxic elements, while possessing similar properties. Copper indium sulfide (CuInS_2 , CIS, bulk band gap: 1.45 eV) NCs show size-dependent photoluminescence (PL) in the red to near infrared spectral window and large absorption coefficients, and are therefore a promising alternative for lead or cadmium chalcogenide NCs in applications such as light-emitting diodes,³⁻⁵ photovoltaics,⁶⁻⁸ luminescent solar concentrators^{9,10} and bio imaging.^{11,12} However, the low PL quantum yields (QYs) of bare CIS NCs (typically below 5%)¹³ preclude their direct application. Improvement of the PL QYs can be achieved by overcoating the CIS NCs with a shell of wide band gap semiconductors, such as ZnS or CdS.^{1,9,14-17} The best results so far have been reported for CIS/CdS core/shell NCs, which show PL QYs up to 86%,^{9,14} while for CIS/ZnS core/shell NCs PL QYs up to 70% have been reported.^{14,18} Alternative strategies to obtain high PL QY CIS-based core/shell NCs employing exclusively cadmium and lead-free materials are desired, but have not yet been devised. To make the next step in the improvement of the PL quantum yield of CIS NCs, a better understanding of the nature of the emitting state and of the prevailing efficiency limiting processes is needed.

Bulk CIS is known for its rich defect chemistry¹⁹⁻²³ and tolerance to stoichiometry deviations,^{21,22,24-27} leading to many intra-band gap states.^{19-21,23} The stoichiometry affects also the optoelectronic properties of nanocrystalline CIS, as copper deficiency has been reported to induce a widening of the band gap.²⁸ While in the well-known lead- and cadmium-chalcogenide NCs (e.g., PbSe and CdSe) the PL originates from radiative recombination of a delocalized electron in the conduction band (CB) with a delocalized hole in the valence band (VB), the origin of PL in CIS NCs is still under debate.^{13,29} A commonly invoked mechanism to explain the intriguing characteristics of the PL of CIS NCs (*viz.*, broad bandwidths of typically ~200-300 meV, long lifetimes of hundreds of nanoseconds and large Stokes shifts of typically ~300-400 meV), is donor-acceptor pair recombination involving native point defects,^{17,28,30-32} which is based on the assumption that the exciton radiative recombination mechanisms in nanoscale and bulk CIS are the same. This model however does not explain the size dependence of the PL energies, which follow the same trend as that observed for the absorption transitions. Other models involve one localized charge carrier, either the electron^{29,33-35} or the hole,^{14,36,37} that radiatively recombines with the remaining delocalized charge carrier. Yet another model was recently proposed, which precludes the involvement of localized carriers, ascribing the PL to the recombination of CB electron states with dark and bright VB hole states.³⁸ Clearly, the optoelectronic properties of CIS NCs are still poorly understood.

In this work we study the charge carrier dynamics in CIS core and core-shell NCs on ps-ns timescales with transient absorption (TA) in the VIS-NIR spectral region and on ns- μ s timescales with PL spectroscopy. We compare bare CIS (core-only) and core/shell CIS/ZnS NCs to high PL QY CIS/CdS NCs. The charge carrier dynamics on timescales between ps and μ s are strongly

correlated with the PL QY. In the TA experiment, we can distinguish between relaxation pathways for electrons and holes. The hole localizes on a Cu-atom on sub-ps timescales, but this does not negatively affect the PL QY. Instead, the QY-determining step is concluded to be electron trapping. This process is rapid in core-only CIS NCs with low PL QY, and inhibited in core-shell architectures leading to higher efficiencies.

RESULTS AND DISCUSSION

The studied CIS core NCs have the chalcopyrite crystal structure and a trigonal pyramidal shape with a base of 2.5 ± 0.4 nm and height of 2.4 ± 0.3 nm (Figure 1A). These NCs have a featureless absorption spectrum extending up to ~ 650 nm and a broad PL peak centered at 660 nm with a full width at half maximum (FWHM) of 300 meV and a Stokes shift of 436 meV (Figure 2A and Supporting Information, Figure S1). The trigonal pyramidal shape of the NCs is preserved after CdS shell overgrowth, while the size increases to a base of 3.1 ± 0.4 nm and height of 3.0 ± 0.3 nm (Figure 1B). This corresponds to a shell thickness of one monolayer. The exact size and shape of the CIS/ZnS core/shell NCs could not be determined, because this sample was not sufficiently clear of excess ligands to be imaged with high-resolution high-angle annular dark field scanning transmission electron microscopy (HAADF-STEM). The PL and absorption spectra shift to higher energies after shell overgrowth, for both ZnS and CdS shells (Figure 2A). A blue shift of the optical transitions is commonly observed after ZnS overcoating of CIS NCs and also in the early stages of CdS shell growth on CIS NCs,¹⁴ but is nevertheless not yet well-understood. The blue shift has been ascribed to alloying,^{15,39-44} size reduction due to cation exchange⁴⁵ or etching,^{14,42,45} interfacial strain,⁴⁶ and surface reconstruction.⁴⁷ Shell overgrowth is

observed to greatly improve the PL QYs, which increase from 2% for the bare CIS core NCs to 29% for CIS/ZnS NCs and 86% for CIS/CdS NCs. At the same time, the PL lifetimes become longer for the more efficient samples (Figure 2B), indicating the existence of non-radiative recombination pathways that are (partially) blocked upon shell growth.^{14,15,40} On the other hand, the Stokes shift and PL bandwidth are hardly affected by the growth of a ZnS or CdS shell (Figure 2 and Supporting Information, Figure S1). The values for the Stokes shift are 436 meV for bare CIS *versus* 408 meV for CIS/ZnS and 392 meV for CIS/CdS, while the PL bandwidths are 300 meV (CIS) *versus* 311 meV (CIS/ZnS) and 328 meV (CIS/CdS). This indicates that the same electronic transitions are visible in the absorption and emission spectra of bare and core/shell CIS NCs.

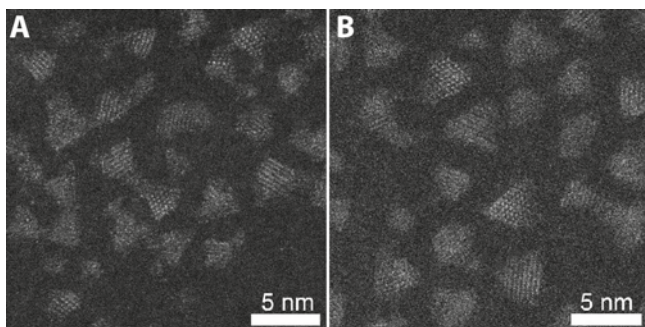


Figure 1. HAADF-STEM images of A) CIS core NCs and B) CIS/CdS core/shell NCs.. The CIS NCs have a base of 2.5 ± 0.4 nm and height of 2.4 ± 0.3 nm, the CIS/CdS core/shell NCs have a base of 3.1 ± 0.4 nm and height of 3.0 ± 0.3 nm.

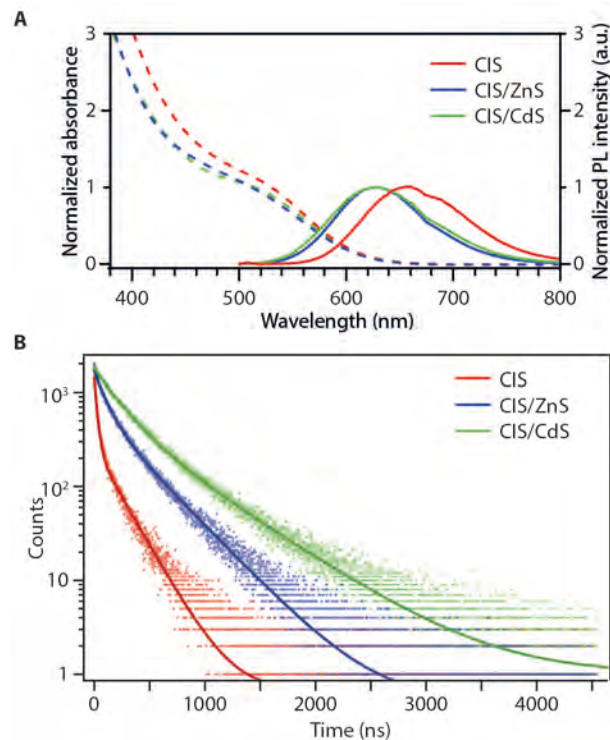


Figure 2. A) Steady state absorption (dashed lines) and PL (solid lines) spectra of CIS NCs (red), CIS/ZnS core/shell NCs (blue) and CIS/CdS core/shell NCs (green). PL excitation spectra are shown in the Supporting Information, Figure S1. B) PL decay curves of the three samples (data points), fitted with a bi-exponential function (solid lines). The fits yield decay constants of 25 and 207 ns for CIS core NCs, 201 and 357 ns for CIS/ZnS NCs, and 209 and 566 ns for CIS/CdS NCs.

Time-resolved transient absorption (TA) spectroscopy allows a closer look on the fast processes that take place in the NCs after excitation and can therefore provide more insight in the fast non-radiative recombination pathways in the NCs. In our TA experiments, the NCs dispersed in hexane are excited with a short (170 fs) pump laser pulse at 500 nm, after which broad-band probe pulses in the range 350 nm – 1600 nm at variable time delay records changes

in the NC absorption spectrum. Figure 3 shows schematically the different processes that can take place. If the pump pulse creates an electron-hole pair in the lowest-energy levels of the conduction and valence bands, the transition between those energy levels is partially blocked (Figure 3A). Therefore, the absorbance at the first absorption transition after photoexcitation with the pump pulse will be lower than the absorbance of the sample with all NCs in the ground state, i.e. prior to excitation. This phenomenon is called the band edge bleach and appears as a negative signal in the TA spectra. If, on the other hand, the photogenerated electron and hole occupy localized energy levels (*e.g.*, a defect or trap level), then the conduction and valence band energy levels remain unoccupied as in the ground state. In this scenario, no difference in absorbance will be observed before and after the pump pulse (Figure 3B). Excited charge carriers can also give rise to additional absorption transitions, in which the already excited carrier is promoted to even higher energy levels (Figure 3C). This can lead to stronger absorption at specific energies compared to the sample in the ground state (Figure 3C), which appear as positive signals in the TA spectra. This phenomenon is called excited state absorption or photo-induced absorption.

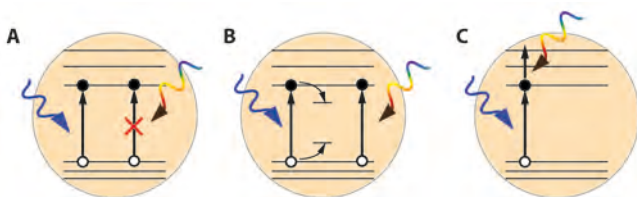


Figure 3. Schematic representation of different processes that can take place in a TA experiment.

A) An exciton in delocalized energy levels blocks the lowest energy transition (band edge bleach). B) If both photogenerated charge carriers localize, the lowest energy transition becomes

available again and no ground state bleach is observed. C) Excited charge carriers can also introduce new absorption transitions, leading to photo-induced absorption.

Figure 4A shows TA spectral slices (2-dimensional TA images are shown in the Supporting Information, Figure S2) for CIS NCs excited by a 500 nm pump pulse for pump-probe delay times between 1 ps and 2 ns. A negative signal around 530 nm is observed, meaning the excited sample absorbs less at these wavelengths than in the ground state. The negative signal is observed at the same energy as the shoulder in the steady state absorption spectrum (Figure 2A), indicating that this is the lowest energy transition (see Supporting Information, Figure S5). The signal is therefore assigned to the ground state bleach, in agreement with previous reports.^{34,36,48–51} At long wavelengths (700 nm – 1600 nm) a broad positive signal is observed. In some studies the high energy tail of this feature was observed as well,^{34,48} but to the best of our knowledge, the present study is the first to measure up to 1600 nm in the near infra-red spectral region, revealing the true magnitude of this TA spectral feature. This positive TA signal is assigned to excited state absorption,^{34,48} and its possible nature will be discussed in more detail below. Both features partially decay on the investigated timescale of 2.5 ns. The TA spectral slices of CIS/ZnS NCs (Figure 4B, 2-dimensional TA images in the Supporting Information, Figure S3) are qualitatively similar to those for the bare CIS cores. Again, we observe a decaying ground state bleach signal at 530 nm and a decaying broad excited state absorption signal. The situation is different in CIS/CdS NCs (Figure 2C, 2-dimensional TA images in the Supporting Information, Figure S4). The ground state bleach and excited state absorption signals are observed as well in the CIS/CdS sample, but they hardly decay on the ns timescale investigated here. The persistent ground state bleach signal excludes the donor-acceptor pair recombination model, as in this scenario both

charge carriers would rapidly be trapped. In this case the bleach due to state filling of the lowest quantum confined energy levels should rapidly decrease. This is clearly in contradiction with our observations.

In recent work by Knowles *et al.*³⁷ and Rice *et al.*⁵² a paramagnetic feature in magnetic circular dichroism spectra and Zeeman splitting in magnetic circularly polarized luminescence spectra of CIS NCs is observed. These features are assigned to the presence of Cu²⁺ ions.^{37,52} Both groups concluded that the PL in CIS NCs originates from radiative recombination of a delocalized electron with a localized hole, in agreement with previous reports.^{14,50} However, based on their observations, the authors were able to propose that the hole is localized, specifically, on a Cu ion.^{37,52} Our observations are consistent with these recent models, since we observe that the decay dynamics of the ground state bleach and of the excited state absorption are different (see Figure 5). In particular, in CIS core and CIS/ZnS core-shell NCs the bleach signal decays faster in the first 100 ps than the excited state absorption. This must mean that the two signals originate from different charge carriers. The ground state bleach observed in our TA data (Figure 4) is predominantly due to the electron in the lowest-energy delocalized conduction band state. Theoretical work carried out by Jaffe and Zunger has shown that the upper VB in ternary copper chalcogenides is composed primarily of Cu 3d orbitals hybridized with the p orbitals of the group VI element (here: S 3p), while the CB consists primarily of Cu 4s orbitals.⁵³ This implies that the degeneracy of the electron (CB) states is much lower than that of the hole (VB) states. The lower degeneracy of the electron states at the band edge leads to a stronger dependence of the TA signal on the population of the electron states. We note that previous work by Li *et al.*¹⁴ has shown that the state responsible for the ground state bleach in the TA spectra of CIS NCs has a twofold degeneracy, thereby being consistent with an electron state. We attribute the excited

state absorption signal to the hole localized on Cu that can absorb lower energy photons. This could be due to interconfigurational d-d transitions on Cu^{2+} or ligand-to-metal charge transfer transitions where the hole is excited to nearby a VB level.⁵⁴ It should be noted that the steady state absorption spectra of all three samples do not show any significant absorption in the 800 - 1600 nm range (Supporting Information, Figure S6). Moreover, laser excitation with sub-band gap energy does not induce any observable TA signal. This implies that localized holes and/or excess carriers are either absent or have negligible concentrations prior to the photogeneration of excitons.

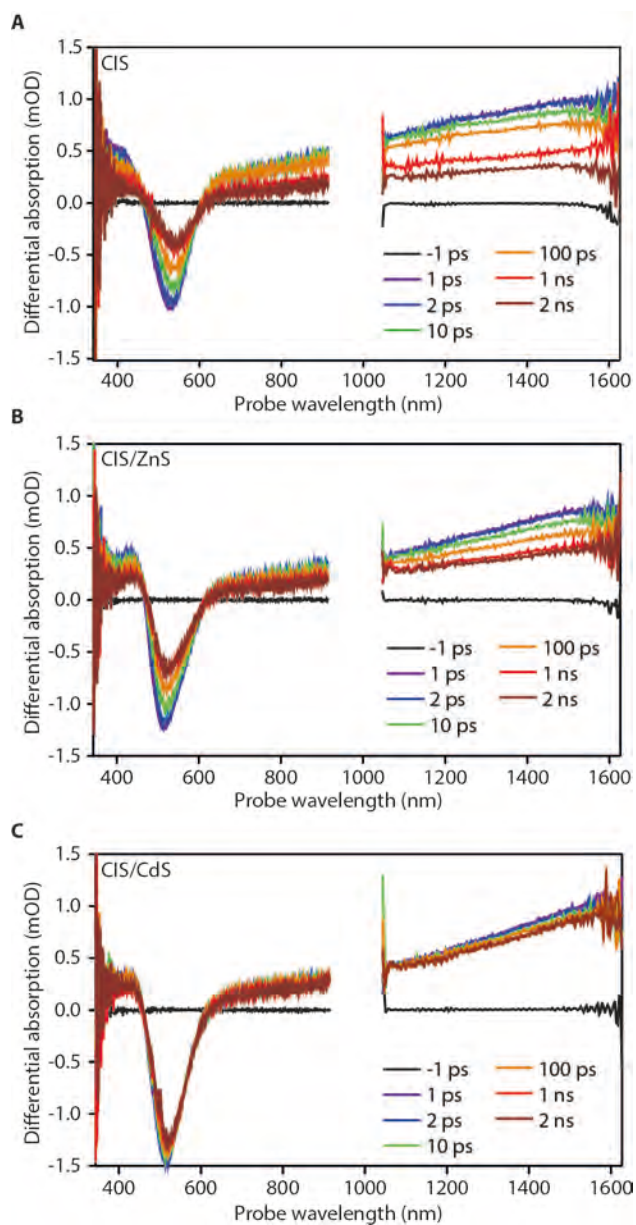


Figure 4. Spectral slices of TA measurements of the three samples (pump wavelength 500 nm, fluence: 2.2×10^{13} photons/cm²): A) CIS NCs, B) CIS/ZnS NCs, C) CIS/CdS NCs. 2D TA spectra are provided in the Supporting Information (Figures S2 – S4). In all three samples a negative ground state bleach signal (around 530 nm) and a broad excited state absorption signal is observed.

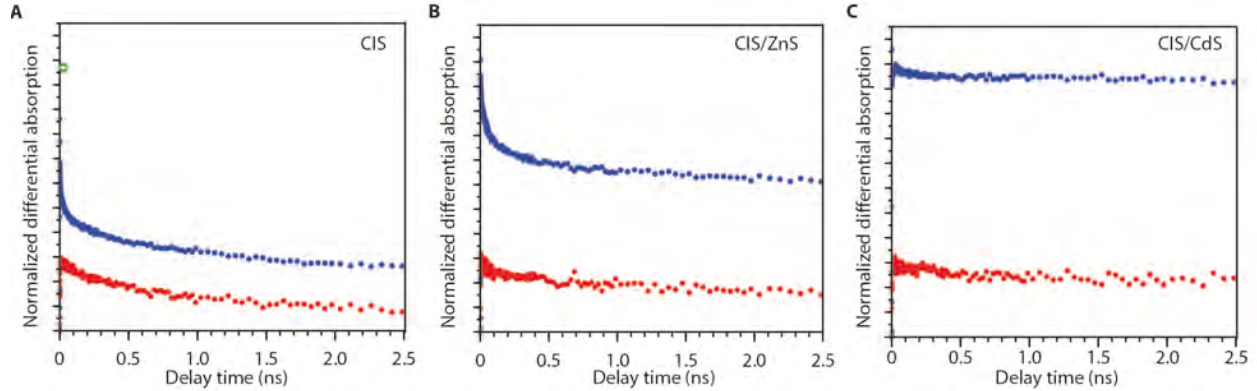


Figure 5. Comparison of the dynamics of the ground state bleach (blue) and excited state absorption (red) signals for the three samples: CIS core NCs (A), CIS/ZnS core/shell NCs (B) and CIS/CdS core/shell NCs (C). Both the excited state absorption and the ground state bleach signal are normalized to the signal amplitude of the excited state absorption at $t = 0$. The green circle in panel A would be the initial amplitude of the ground state blue in the absence of ultrafast electron trapping (see main text below for a discussion).

The TA decay dynamics of the three samples are shown in Figure 6A-C. With an excitation power of 4.9 mW, corresponding to a fluence of 2.2×10^{13} photons/cm², we are in the linear regime where the TA experiment does not depend on laser fluence, with an estimated number of excitons per NC of $\langle N_0 \rangle = 0.03$ (see Supporting Information, Figures S7 and S8, for power dependent TA spectra and calculation). In the analysis, we can therefore neglect effects of Auger recombination of multi-exciton states. We plot the dynamics of the ground state bleach, sensitive to the electron population in the lowest-energy conduction band state, in blue. The dynamics of the excited state absorption, proportional to the population of localized holes, are given in red. Overall, there is a trend of slower dynamics for samples with higher PL efficiency, proving that the non-radiative recombination pathways affect ps-ns dynamics as well as ns- μ s dynamics (see

Figure 2 above). The initial intensity at $t = 0$ of the ground state bleach signal (blue) relative to the excited state absorption signal (red) is lower in CIS core NCs than in the two other samples. Since the transitions probed are the same for the three samples (as demonstrated by the identical TA spectra), the relative signal strengths should also be the same. Therefore, the lower ground state bleach signal in CIS NCs points to ultrafast electron trapping in some NCs on sub-ps time scales that cannot be resolved in the TA experiment; e.g. because electrons are trapped from hot-electron states. Without ultrafast electron trapping, the bleach in CIS QDs at $t = 0$ would be at the green circle in Figure 6A.

Figure 5 shows that the dynamics of the electron (blue) and hole (red) populations are notably different on the ps timescale. The electron population decays more rapidly in CIS and CIS/ZnS than the hole population. However, the intensity ratio of electron and hole signals at a delay time of 3 ns is the same for the three samples (see Fig. 5A-C). This means that the decay pathways of electron and hole are separate on a ps timescale, but eventually coupled on a ns timescale. Indeed, For CIS/ZnS, the electron and hole populations drop by 44% and 41% over the first 3 ns, respectively, and in CIS/CdS by 4% and 4%. In CIS core NCs, the drops in electron and hole population are also consistent if we take into account the effect of ultrafast electron trapping (see discussion above). The drop in electron population in CIS core NCs is then 78% over 3 ns (counted from the green point at $t = 0$) *versus* 72% for the hole population. We conclude that the overall decay of electron and hole population over 3 ns must be due to recombination (radiative and/or non-radiative), which explains why the signal ratio at 3 ns is the same for the three samples. We ascribe the fast ps dynamics of the bleach signal in CIS to CIS/ZnS to trapping of CB electrons. Indeed, trapping of the CB electron would make it unobservable in our TA experiment, while this process does not immediately affect the hole population. Subsequently,

trapped electrons recombine non-radiatively with the hole on a ns timescale, leading to the observation of coupled populations eventually. Interestingly, the drops in population over 3 ns correlate well with the PL quantum yields of the samples, confirming that the sub-ns charge carrier dynamics reflect non-radiative recombination pathways.

We now use our observations and analysis to build a simple kinetic model (Figure 6D) for the charge carrier dynamics and non-radiative recombination pathway in CIS NCs. It involves ultrafast (sub-ps) localization of the hole, as evidenced by the absence of a rise in the excited state absorption signal. Likewise, the electron reaches the lowest conduction band state on sub-ps time-scales. The resulting situation is schematically depicted in Figure 6D, state II. In some NCs, the electron is subsequently trapped on ps-ns timescales, giving rise to a fast component in the ground state bleach decay dynamics, resulting in state III in Figure 6D. A trapped electron recombines non-radiatively with the localized hole, resulting in the ~ns decay dynamics of the photo induced absorption (process III to IV). When the electron is not trapped it recombines radiatively with the localized hole (process II to IV) on ns- μ s time scales.

Our model matches the observed TA dynamics for all three samples well. The solid lines in Figure 6A–C are the result of a global fit of the TA dynamics of the three samples (see Supporting Information for details). The good match confirms that electron trapping is the first step in the non-radiative recombination pathway in CIS-based NCs (states II to III in Figure 6D). Indeed, the global fit reproduces the differences between the three samples by keeping all parameters fixed except the rates of electron trapping. The differences in hole dynamics for the three samples are a secondary effect, effectuated by non-radiative recombination of the hole with the trapped electron (states III to IV). The non-radiative decay has a fixed rate of 1/(904 ps) for the three samples, but the probability that it occurs varies according to the electron trapping rate.

This means that electron trapping is the primary cause for non-radiative recombination in CIS-based NCs. The model presented here is applied to the measurement with 500 nm laser excitation pulse with a fluence of 2.2×10^{13} photons/cm². In the Supporting Information we show the model fitted to a measurement on the same NCs, using a 400 nm laser excitation pulse with a fluence of 6.9×10^{12} photons/cm².

The dynamical model presented here provides important new insights into the *non-radiative* decay pathways of electrons and holes in CIS-based NCs. At the same time, it confirms recent propositions for the nature of *radiative* decay in these NCs.^{37,52} Radiative decay (state II to state IV in Figure 6D) is due to recombination of a hole localized on a Cu ion with a CB electron. This naturally explains the intriguing characteristics of PL in CIS-based NCs. Radiative lifetimes are long (see Figure 2B) because the wave function overlap of a delocalized CB electron with a localized hole is relatively small. Furthermore, the large Stokes shift and broad emission bands are due to coupling to vibrations. Indeed, strong vibrational coupling is expected for transitions with a charge-transfer character (the localized hole effectively oxidizes a Cu⁺ ion to Cu²⁺), because they are accompanied by changes in metal-to-ligand bond length.⁵⁵

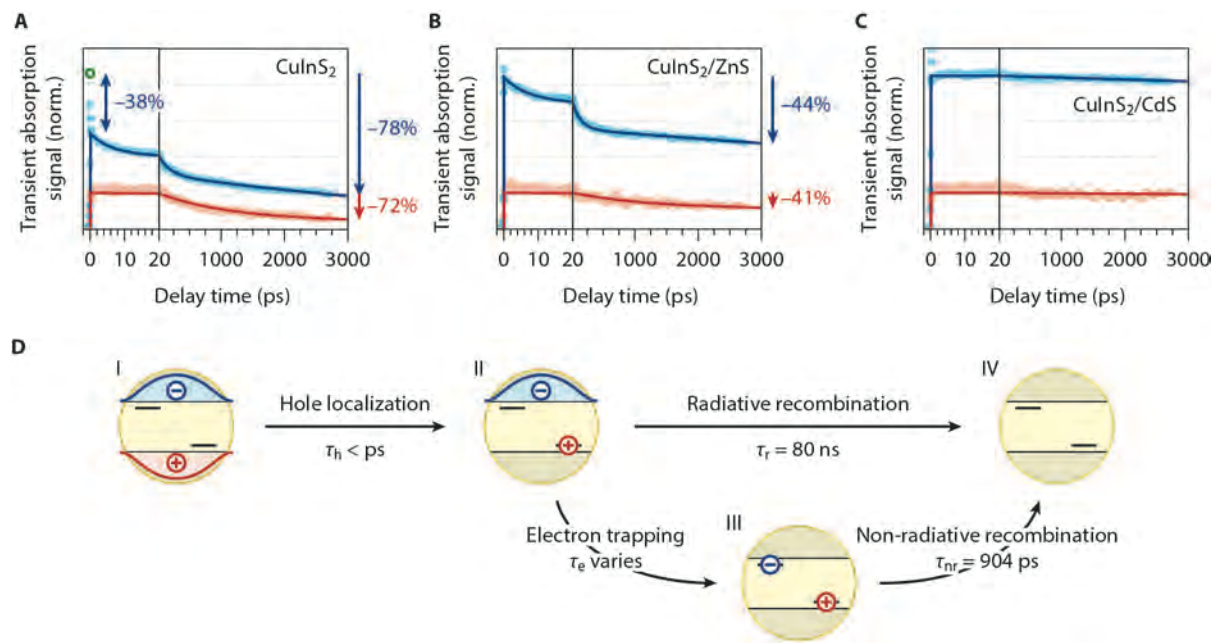


Figure 6. A, B, C) decay dynamics of the TA signals, in blue the ground state bleach signal, in red the excited state absorption. The solid lines are fits of our model to the lighter colored data points. Both the excited state absorption (red) and the ground state bleach (blue) are normalized to the signal amplitude of the excited state absorption (red) at $t = 0$. The green circle in panel A would be the initial amplitude of the ground state blue in the absence of ultrafast electron trapping (see main text for a discussion). D) Schematic representation of the model proposed. After photoexcitation creating an exciton, there is a fast localization of the hole. A distribution of electron trapping rates makes the TA signal decay multiexponential. A trapped electron recombines non-radiatively with the localized hole, while a delocalized electron recombines radiatively with the localized hole. The fitted “radiative lifetime” of 80 ns, based on the data on CIS/CdS NCs, is a rough estimate, and cannot be determined accurately because our TA experiment has a too short time range (see also Figure 2). The fitted time constants for electron trapping are 6 ps (with a contribution of 21%), 174 ps (21%) and 6.5 ns (58%) for CIS core NCs, and 6 ps (14%), 129 ps (20%) and 19 ns (66%) for CIS/ZnS. The time constant for non-radiative

recombination of the trapped electron with a localized hole is 904 ps, obtained from a global fit to the excited state absorption transients. The ratio of excited state absorption and ground state bleach cross-sections is 0.24. See the Supporting Information for more details of the model and the fitting procedure.

The results presented above show that electron trapping leading to non-radiative decay is most effectively blocked by growing a CdS shell around CIS NCs. The differences between the two shell materials used in this study are both electronic and structural. When combining the information on band potentials given by Van de Walle *et al.*⁵⁶ and Hunger *et al.*,⁵⁷ a type I band alignment is expected for CIS/ZnS core/shell heteronanocrystals, confining both charge carriers in the core, while a type II band alignment is expected for CIS/CdS core/shell heteronanocrystals, spatially separating the electron (in the CdS shell) and hole (in the CIS core). However, the shells used in the present study are too thin (*viz.*, 1 monolayer) to significantly affect the carrier localization regime, and therefore their impact on the electron recombination pathways most likely results from differences in their ability to eliminate electron traps at the CIS surface. The lattice mismatch is 2% between CIS and ZnS (lattice parameters $a, b = 5.52279$ Å for CIS,⁵⁸ lattice parameters $a, b, c = 5.41450$ Å for ZnS⁵⁹), and 5.2% between CIS and CdS (lattice parameters $a, b, c = 5.81000$ for CdS⁶⁰). The small lattice mismatch between CIS and ZnS, in combination with the high diffusion rates in CIS,⁶¹ might favor interdiffusion and alloy formation, which would result in some surface Cu and In atoms, thereby preventing the complete elimination of CIS-related surface traps. In contrast, the larger mismatch between CIS and CdS would prevent interdiffusion, facilitating the formation of a CIS/CdS core/shell architecture, in which the surface of the NCs would be devoid of CIS units and therefore of CIS-related surface traps.

CONCLUSION

In conclusion, we have carried out a detailed analysis of the TA dynamics of the ground state bleach and excited state absorption signals of CIS core NCs, CIS/ZnS core/shell NCs and CIS/CdS core/shell NCs. Based on this analysis we propose a model that describes two exciton recombination pathways in CIS and CIS-based NCs, one leading to non-radiative decay, the other to radiative decay. The radiative decay originates from recombination of a delocalized electron to a localized hole. The difference in energy between the highest energy level in the valence band and the localized hole state explains the large Stokes shift. The exact energy level of the localized hole depends on the position of the Cu ion in the crystal lattice and this thus leads to broad a PL peak. Because the hole is localized, the wave functions of the electron and hole overlap less compared to two delocalized carriers. This leads to long PL decay times. Electron trapping, probably on the surface of the CIS NCs, is the first step of the non-radiative recombination pathway. Removing these traps leads to improvement of the PL QY of CIS-based core/shell NCs.

METHODS

Materials. Copper (I) iodide (Sigma Aldrich, 98%), Indium (III) acetate (Sigma Aldrich, 99.99%), 1-dodecanethiol (DDT, Sigma Aldrich, $\geq 98\%$), Trioctylphosphine (TOP, Fisher Scientific), Zinc (II) stearate (Sigma Aldrich, 10-12% Zn basis), Cadmium (II) oxide (Sigma Aldrich, 99.5%), Oleic Acid (Oleic acid, OA, Sigma Aldrich, 90%), 1-octadecene (ODE, Sigma

Aldrich, tech. 90%), Sulfur (Sigma Aldrich, 99.98%), Oleylamine (OLAM, Sigma Aldrich, tech. 70%), Toluene (Sigma Aldrich, 99.8%), Acetone (VWR International bv, dried, max. 0.0075% H₂O). Methanol (Sigma Aldrich, 99.8%), 1-Butanol (Sigma Aldrich, 99.8%), Hexane (Sigma Aldrich, anhydrous, 95%). ODE and OLAM were degassed at for 2 hours at 150-220 °C before usage.

CIS nanocrystals. For the synthesis of the CIS core NCs a protocol by Li *et al.*¹⁴ was followed. 297 mg In(Ac)₃, 191 mg CuI, and 5 mL DDT were mixed and degassed for one hour at 80 °C. Then the reaction mixture was heated under N₂ flow to 230 °C and allowed to react for 5 minutes. Part of the solution that was not needed for shell synthesis was washed with acetone and dispersed in toluene.

CIS/ZnS core/shell nanocrystals. For the synthesis of the CIS/ZnS core/shell NCs a protocol by Li *et al.*¹⁴ was followed. 1 mL of the crude CIS reaction mixture was diluted with 4 mL ODE and degassed for 30 minutes at 80 °C. 259 mg Zn-stearate, 4 mL ODE and 0.4 mL sulfur dissolved in TOP were mixed and heated to 200 °C to dissolve the Zn-stearate. The CIS solution was heated to 210 °C under N₂ flow and the mixture with zinc and sulfur was added dropwise over 20 minutes. After addition the mixture was allowed to react for 20 minutes at 210 °C. Then the mixture was cooled to room temperature, washed with acetone and dispersed in toluene.

CIS/CdS core/shell nanocrystals. For the synthesis of the CIS/CdS core/shell NCs a protocol by Li *et al.*¹⁴ was followed. A 0.38 M Cd-oleate solution was made by dissolving 383 mg CdO in 3.9 mL oleic acid and 3.9 mL ODE at 280 °C under N₂ flow. After 1 hour the CdO was dissolved and the solution was degassed for 30 minutes at 110 °C. 1 mL of the crude CIS reaction mixture was diluted with 4 mL ODE and degassed for 30 minutes at 80 °C. 4 mL ODE, 1 mL Cd-oleate solution and 0.4 mL 1 M sulfur in TOP solution were mixed. The CIS solution was heated to 210

°C under N₂ flow and the mixture with cadmium and sulfur was added dropwise over 20 minutes. After addition the mixture was allowed to react for 20 minutes at 210 °C. Then the mixture was cooled to room temperature, washed with acetone and dispersed in toluene.

Electron microscopy. HAADF-STEM images were acquired on a ...Eva, please complete

PL quantum yield. The PL quantum yield of the three samples was determined using the fluorophore Lumogen red 350 with PL QY of 95% as reference. Samples for PL QY measurements were prepared by diluting the stock solution of washed NCs with anhydrous toluene under nitrogen in sealed quartz cuvettes. Lumogen red 350 was dissolved in toluene as well. The absorption and PL emission spectra were measured at equipment as listed below. The PL QY was calculated using the following equation: $QY = (1 - T_{ref}) / (1 - T) \times \Phi / \Phi_{ref} \times QY_{ref}$, in which T is the transmission at 400 nm and Φ is the area under the PL emission peak.⁶²

Steady state optical spectroscopy. Samples for optical measurements were prepared by diluting the stock solution of washed NCs with anhydrous toluene under nitrogen and stored in sealed quartz cuvettes. Absorption spectra were measured on a double-beam PerkinElmer Lambda 16 UV/vis spectrometer. Photoluminescence emission spectra were recorded on an Edinburgh Instruments FLS920 spectrofluorimeter equipped with a 450W xenon lamp as excitation source and double excitation monochromator with a grating blazed at 300 nm. The signal was detected with a Hamamatsu R928 PMT detector with a monochromator with a grating blazed at 500 nm.

Time resolved PL spectroscopy. Samples for time resolved PL spectroscopy were prepared by diluting the stock solution of washed NCs with anhydrous toluene under nitrogen, and stored in sealed quartz cuvettes. PL decay curves were obtained by time-correlated single-photon counting on a Hamamatsu photosensor module H10720-01. A pulsed diode laser (EPL-445 Edinburgh

Instruments, 441 nm, 55 ps pulse width, 0.2 MHz repetition rate) was used as the excitation source. Lifetimes were obtained from a bi-exponential fit of the decay curve.

Transient absorption spectroscopy. The NCs were washed with a 1:1 Methanol:Butanol mixture and dispersed in hexane. The NC dispersions were stored in 1 mm quartz cuvettes and studied using broadband pump-probe spectroscopy.

A Yb:KGW oscillator (Light Conversion, Pharos SP) was used to generate 170 fs laser pulses at 1028 nm. After amplification the majority of the fundamental 1028 nm laser beam underwent nonlinear frequency mixing in an OPA and second harmonics module (Light Conversion, Orpheus) to create the pump laser pulses of 400 and 500 nm. A small fraction of the fundamental 1028 nm beam was used to generate the broadband probe spectrum in a CaF₂ (350 – 650 nm) or sapphire (500 – 1600 nm) crystal and delayed up to 3 ns using an automated delay stage. The NC dispersions were hit by the pump and probe pulses under an angle of ~8° after which the probe pulse is collected on a detector suitable for the probe spectrum generated (Ultrafast Systems, Helios). All TA data shown is corrected for dispersion in the probe light by fitting a polynomial function to the solvent response.

ASSOCIATED CONTENT

Supporting Information. 2D TA images of CIS core NCs, CIS/ZnS core/shell NCs and CIS/CdS core/shell NCs, TA, steady state absorption and PL spectra in one image, steady state absorption spectra of NC solutions as measured with TA, power dependent ground state bleach decay curves and fits of the three samples, power dependent ground state bleach decay curves normalized, calculation of the average number of excitons per NC, model description and global fit details. This material is available free of charge via the Internet at <http://pubs.acs.org>.

AUTHOR INFORMATION

Corresponding Author

*E-mail: c.demello-donega@uu.nl

Present Addresses

§ Freddy T. Rabouw is currently working at Department of Mechanical and Process Engineering, ETH Zürich, Leonhardstrasse 21, 8092 Zürich, Switzerland

Author Contributions

The manuscript was written through contributions of all authors. All authors have given approval to the final version of the manuscript.

ACKNOWLEDGMENT

The authors thank Chenghui Xia for providing the fluorophore Lumogen red 305 for the PL QY measurements. A.C.B. and C.d.M.D. acknowledge financial support from the division of Chemical Sciences (CW) of The Netherlands Organization for Scientific Research (NWO) under grant number ECHO.712.014.001. This research was supported by the Dutch Foundation for Fundamental Research on Matter (FOM) in the program “Hot Electrons in Cool Nanocrystals”.

REFERENCES

- (1) de Mello Donegá, C. Synthesis and Properties of Colloidal Heteronanocrystals. *Chem. Soc. Rev.* **2011**, *40*, 1512–1546.

- (2) Kovalenko, M. V.; Manna, L.; Cabot, A.; Hens, Z.; Talapin, D. V.; Kagan, C. R.; Klimov, X. V. I.; Rogach, A. L.; Reiss, P.; Milliron, D. J.; *et al.* Prospects of Nanoscience with Nanocrystals. *ACS Nano* **2015**, *9*, 1012–1057.
- (3) Yoon, H. C.; Oh, J. H.; Ko, M.; Yoo, H.; Do, Y. R. Synthesis and Characterization of Green Zn–Ag–In–S and Red Zn–Cu–In–S Quantum Dots for Ultrahigh Color Quality of Down-Converted White LEDs. *ACS Appl. Mater. Interfaces* **2015**, *7*, 7342–7350.
- (4) Demir, N.; Oner, I.; Varlikli, C.; Ozsoy, C.; Zafer, C. Efficiency Enhancement in a Single Emission Layer Yellow Organic Light Emitting Device: Contribution of CIS/ZnS Quantum Dot. *Thin Solid Films* **2015**, *589*, 153–160.
- (5) Park, S. H.; Hong, A.; Kim, J.-H.; Yang, H.; Lee, K.; Jang, H. S. Highly Bright Yellow-Green-Emitting CuInS₂ Colloidal Quantum Dots with Core/Shell/Shell Architecture for White Light-Emitting Diodes. *ACS Appl. Mater. Interfaces* **2015**, *7*, 6764–6771.
- (6) Chang, J.-Y.; Su, L.-F.; Li, C.-H.; Chang, C.-C.; Lin, J.-M. Efficient “green” Quantum Dot-Sensitized Solar Cells Based on Cu₂S–CuInS₂–ZnSe Architecture. *Chem. Commun.* **2012**, *48*, 4848.
- (7) Pan, Z.; Mora-Sero, I.; Shen, Q.; Zhang, H.; Li, Y.; Zhao, K.; Wang, J.; Zhong, X.; Bisquert, J. High-Efficiency “green” quantum Dot Solar Cells. *J. Am. Chem. Soc.* **2014**, *136*, 9203–9210.
- (8) Dunst, S.; Rath, T.; Reichmann, A.; Chien, H.; Friedel, B.; Trimmel, G. A Comparison of Copper Indium Sul Fi de-Polymer Nanocomposite Solar Cells in Inverted and Regular Device Architecture. *Synth. Met.* **2016**.

- (9) Knowles, K. E.; Kilburn, T. B.; Alzate, D. G.; McDowall, S.; Gamelin, D. R. Bright CuInS₂/CdS Nanocrystal Phosphors for High-Gain Full-Spectrum Luminescent Solar Concentrators. *Chem. Commun.* **2015**, *51*, 9129–9132.
- (10) Meinardi, F.; McDaniel, H.; Carulli, F.; Colombo, A.; Velizhanin, K. a.; Makarov, N. S.; Simonutti, R.; Klimov, V. I.; Brovelli, S. Highly Efficient Large-Area Colourless Luminescent Solar Concentrators Using Heavy-Metal-Free Colloidal Quantum Dots. *Nat. Nanotechnol.* **2015**.
- (11) Guo, W.; Sun, X.; Jacobson, O.; Yan, X.; Min, K.; Srivatsan, A.; Niu, G.; Kieseewetter, D. O.; Chang, J.; Chen, X.; *et al.* Intrinsically Radioactive [64Cu]CuInS / ZnS Quantum Dots for PET and Optical Imaging□: Improved Radiochemical Stability and Cerenkov Luminescence. *ACS Nano* **2015**, *9*, 488–495.
- (12) Chen, C.-W.; Wu, D.-Y.; Chan, Y.-C.; Lin, C. C.; Chung, P.-H.; Hsiao, M.; Liu, R.-S. Evaluations of the Chemical Stability and Cytotoxicity of CuInS₂ and CuInS₂/ZnS Core/Shell Quantum Dots. *J. Phys. Chem. C* **2015**, *119*, 2852–2860.
- (13) van der Stam, W.; Berends, A. C.; de Mello Donegá, C. Prospects of Colloidal Copper Chalcogenide Nanocrystals. *ChemPhysChem* **2015**, 559–581.
- (14) Li, L.; Pandey, A.; Werder, D. J.; Khanal, B. P.; Pietryga, M.; Klimov, V. I. Efficient Synthesis of Highly Luminescent Copper Indium Sulfide-Based Core/Shell Nanocrystals with Surprisingly Long-Lived Emission. *J. Am. Chem. Soc.* **2011**, *133*, 1176–1179.
- (15) Trizio, L. De; Prato, M.; Genovese, A.; Casu, A.; Povia, M.; Simonutti, R.; Alcocer, M. J. P.; Andrea, C. D.; Tassone, F.; Manna, L. Strongly Fluorescent Quaternary Cu – In – Zn

- S Nanocrystals Prepared from Cu_{1-x}InS₂ Nanocrystals by Partial Cation Exchange. *Chem. Mater.* **2012**, *24*, 2400–2406.
- (16) Feng, J.; Sun, M.; Yang, X. A Facile Approach to Synthesize High-Quality Zn_xCu_yInS_{1.5+x+0.5y} Nanocrystal Emitters. *Chem. Commun. (Camb)*. **2011**, Supporting.
- (17) Seo, J.; Raut, S.; Abdel-Fattah, M.; Rice, Q.; Tabibi, B.; Rich, R.; Fudala, R.; Gryczynski, I.; Gryczynski, Z.; Kim, W.-J.; *et al.* Time-Resolved and Temperature-Dependent Photoluminescence of Ternary and Quaternary Nanocrystals of CuInS₂ with ZnS Capping and Cation Exchange. *J. Appl. Phys.* **2013**, *114*, 094310.
- (18) Kim, Y.-K.; Ahn, S.-H.; Chung, K.; Cho, Y.-S.; Choi, C.-J. The Photoluminescence of CuInS₂ Nanocrystals: Effect of Non-Stoichiometry and Surface Modification. *J. Mater. Chem.* **2012**, *22*, 1516.
- (19) Ueng, H. Y.; Hwang, H. . The Defect Structure of CuInS₂. Part I: Intrinsic Defects. *J. Phys. Chem. Solids* **1989**, *50*, 1297–1305.
- (20) Lewerenz, H. J.; Dietz, N. Defect Identification in Semiconductors by Brewster Angle Spectroscopy. *J. Appl. Phys.* **1993**, *73*, 4975–4987.
- (21) Zhang, S. B.; Wei, S.-H.; Zunger, A.; Katayama-Yoshida, H. Defect Physics of the CuInSe₂ Chalcopyrite Semiconductor. *Phys. Rev. B* **1998**, *57*, 9642–9656.
- (22) Perniu, D.; Duta, A.; Schoonman, J. The Defect Structure of Copper Indium Disulfide. *Funct. Nanoscale Mater. Devices Syst.* **2008**, 457–464.
- (23) Binsma, J. J. M.; Giling, L. J.; Bloem, J. Luminescence of CuInS₂. II Exciton and near

- Edge Emission. *J. Lumin.* **1982**, 55–72.
- (24) Verheijen, A. W.; Giling, L. J.; Bloem, J. The Region of Existence of CuInS₂. *Mater. Res. Bull.* **1979**, *14*, 237–240.
- (25) Fearheiley, M. L. The Phase Relations in the Cu,In,Se System and the Growth of CuInSe₂ Single Crystals. *Sol. Cells* **1986**, *16*, 91–100.
- (26) Binsma, J. J. .; Giling, L. J.; Bloem, J. Phase Relations in the System Cu₂-S-In₂S₃. *J. Cryst. Growth* **1980**, *50*, 429–436.
- (27) Hsu, T. M. Study of CuInS₂ Grown by the Travelingheater Method by Electrolyte Electroreflectance. *J. Appl. Phys.* **1986**, *59*, 2538–2540.
- (28) Chen, B.; Zhong, H.; Zhang, W.; Tan, Z.; Li, Y.; Yu, C.; Zhai, T.; Bando, Y.; Yang, S.; Zou, B. Highly Emissive and Color-Tunable CuInS₂-Based Colloidal Semiconductor Nanocrystals: Off-Stoichiometry Effects and Improved Electroluminescence Performance. *Adv. Funct. Mater.* **2012**, *22*, 2081–2088.
- (29) Leach, A. D. P.; Macdonald, J. E. The Optoelectronic Properties of CuInS₂ Nanocrystals and Their Origin. *J. Phys. Chem. Lett.* **2016**, acs.jpcclett.5b02211.
- (30) Zhong, H.; Zhou, Y.; Ye, M.; He, Y.; Ye, J.; He, C.; Yang, C.; Li, Y. Controlled Synthesis and Optical Properties of Colloidal Ternary Chalcogenide CuInS₂ Nanocrystals. *Chem. Mater.* **2008**, *20*, 6434–6443.
- (31) Castro, S. L.; Bailey, S. G.; Raffaele, R. P.; Banger, K. K.; Hepp, A. F. Synthesis and Characterization of Colloidal CuInS₂ Nanoparticles from a Molecular Single-Source

- Precursor. *J. Phys. Chem. B* **2007**, *108*, 12429–12435.
- (32) Nam, D. E.; Song, W. S.; Yang, H. Noninjection, One-Pot Synthesis of Cu-Deficient CuInS₂/ZnS Core/shell Quantum Dots and Their Fluorescent Properties. *J. Colloid Interface Sci.* **2011**, *361*, 491–496.
- (33) Omata, T.; Nose, K.; Kurimoto, K.; Kita, M. Electronic Transition Responsible for Size-Dependent Photoluminescence of Colloidal CuInS₂ Quantum Dots. *J. Mater. Chem. C* **2014**, *2*, 6867.
- (34) Kraatz, I. T.; Booth, M.; Whitaker, B. J.; Nix, M. G. D.; Critchley, K. Sub-Bandgap Emission and Intraband Defect-Related Excited-State Dynamics in Colloidal CuInS₂/ZnS Quantum Dots Revealed by Femtosecond Pump – Dump – Probe Spectroscopy. *J. Phys. Chem. C* **2014**, *118*, 21102–24109.
- (35) Hamanaka, Y.; Kuzuya, T.; Sofue, T.; Kino, T.; Ito, K.; Sumiyama, K. Defect-Induced Photoluminescence and Third-Order Nonlinear Optical Response of Chemically Synthesized Chalcopyrite CuInS₂ Nanoparticles. *Chem. Phys. Lett.* **2008**, *466*, 176–180.
- (36) Cadirci, M.; Masala, O.; Pickett, N.; Binks, D. Ultrafast Charge Dynamics in CuInS₂ Nanocrystal Quantum Dots. *Chem. Phys.* **2014**, *438*, 60–65.
- (37) Knowles, K. E.; Nelson, H. D.; Kilburn, T. B.; Gamelin, D. R. Singlet–Triplet Splittings in the Luminescent Excited States of Colloidal Cu⁺:CdSe, Cu⁺:InP, and CuInS₂ Nanocrystals: Charge-Transfer Configurations and Self-Trapped Excitons. *J. Am. Chem. Soc.* **2015**, *137*, 13138–13147.
- (38) Shabaev, A.; Mehl, M. J.; Efros, A. L. Energy Band Structure of CuInS₂ and Optical

- Spectra of CuInS₂ Nanocrystals. *Phys. Rev. B* **2015**, *92*, 035431.
- (39) Feng, J.; Sun, M.; Yang, F.; Yang, X. A Facile Approach to Synthesize High-Quality Zn_(x)Cu_(y)InS_(1.5+x+0.5y) Nanocrystal Emitters. *Chem. Commun. (Camb)*. **2011**, *47*, 6422–6424.
- (40) Huang, L.; Zhu, X.; Publicover, N. G.; Hunter, K. W.; Ahmadiantehrani, M.; de Bettencourt-Dias, A.; Bell, T. W. Cadmium and Zinc Alloyed Cu-In-S Nanocrystals and Their Optical Properties. *J. nanoparticle Res.* **2013**, *15*, 2056.
- (41) Kim, H.; Han, J. Y.; Kang, D. S.; Kim, S. W.; Jang, D. S.; Suh, M.; Kirakosyan, A.; Jeon, D. Y. Characteristics of CuInS₂/ZnS Quantum Dots and Its Application on LED. *J. Cryst. Growth* **2011**, *326*, 90–93.
- (42) Choi, H. S.; Kim, Y.; Park, J. C.; Oh, M. H.; Jeon, D. Y.; Nam, Y. S. Highly Luminescent, off-Stoichiometric Cu_xIn_yS₂/ZnS Quantum Dots for near-Infrared Fluorescence Bio-Imaging. *RSC Adv.* **2015**, *5*, 43449–43455.
- (43) Uehara, M.; Watanabe, K.; Tajiri, Y.; Nakamura, H.; Maeda, H. Synthesis of CuInS₂ Fluorescent Nanocrystals and Enhancement of Fluorescence by Controlling Crystal Defect. *J. Chem. Phys.* **2008**, *129*, 134709.
- (44) Nose, K.; Soma, Y.; Omata, T.; Otsuka-Yao-Matsuo, S. Synthesis of Ternary CuInS₂ Nanocrystals; Phase Determination by Complex Ligand Species. *Chem. Mater.* **2009**, *21*, 2607–2613.
- (45) Park, J.; Kim, S.-W. CuInS₂/ZnS Core/shell Quantum Dots by Cation Exchange and Their Blue-Shifted Photoluminescence. *J. Mater. Chem.* **2011**, *21*, 3745.

- (46) Kim, Y.-K.; Ahn, S.-H.; Choi, G.-C.; Chung, K.-C.; Cho, Y.-S.; Choi, C.-J. Photoluminescence of CuInS₂/(Cd,Zn)S Nanocrystals as a Function of Shell Composition. *Trans. Electr. Electron. Mater.* **2011**, *12*, 218–221.
- (47) Li, L.; Daou, T. J.; Texier, I.; Kim Chi, T. T.; Liem, N. Q.; Reiss, P. Highly Luminescent CuInS₂/ZnS Core/Shell Nanocrystals: Cadmium-Free Quantum Dots for In Vivo Imaging. *Chem. Mater.* **2009**, *21*, 2422–2429.
- (48) Bose, R.; Ahmed, G. H.; Alarousu, E.; Parida, M. R.; Abdelhady, A. L.; Bakr, O. M.; Mohammed, O. F. Direct Femtosecond Observation of Charge Carrier Recombination in Ternary Semiconductor Nanocrystals: The Effect of Composition and Shelling. *J. Phys. Chem. C* **2015**, *119*, 3439–3446.
- (49) Debnath, T.; Maiti, S.; Maity, P.; Ghosh, H. N. Subpicosecond Exciton Dynamics and Biexcitonic Feature in Colloidal CuInS₂ Nanocrystals: Role of In–Cu Antisite Defects. *J. Phys. Chem. Lett.* **2015**, *6*, 3458–3465.
- (50) Sun, J.; Zhu, D.; Zhao, J.; Ikezawa, M.; Wang, X.; Masumoto, Y. Ultrafast Carrier Dynamics in CuInS₂ Quantum Dots. *Appl. Phys. Lett.* **2014**, *104*, 023118.
- (51) Sakamoto, M.; Chen, L.; Okano, M.; Tex, D. M.; Kanemitsu, Y.; Teranishi, T. Photoinduced Carrier Dynamics of Nearly Stoichiometric Oleylamine-Protected Copper Indium Sulfide Nanoparticles and Nanodisks. *J. Phys. Chem. C* **2015**, *119*, 11100–11105.
- (52) Rice, W. D.; Mcdaniel, H.; Klimov, V. I.; Crooker, S. A. Magneto-Optical Properties of CuInS₂ Nanocrystals. *J. Phys. Chem. Lett.* **2014**, *5*, 4105–4109.
- (53) Jaffe, J.; Zunger, A. Electronic Structure of the Ternary Chalcopyrite Semiconductors

- CuAlS₂, CuGaS₂, CuInS₂, CuAlSe₂, CuGaSe₂, and CuInSe₂. *Phys. Rev. B* **1983**, 28, 5822–5847.
- (54) Knowles, K. E.; Hartstein, K. H.; Kilburn, T. B.; Marchioro, A.; Nelson, H. D.; Whitham, P. J.; Gamelin, D. R. Luminescent Colloidal Semiconductor Nanocrystals Containing Copper: Synthesis, Photophysics, and Applications. *Chem. Rev.* **2016**, acs.chemrev.6b00048.
- (55) de Jong, M.; Seijo, L.; Meijerink, A.; Rabouw, F. T. Resolving the Ambiguity in the Relation between Stokes Shift and Huang–Rhys Parameter. *Phys. Chem. Chem. Phys.* **2015**, 17, 16959–16969.
- (56) Van de Walle, C. G.; Neugebauer, J. Universal Alignment of Hydrogen Levels in Semiconductors, Insulators and Solutions. *Nature* **2003**, 423, 626–628.
- (57) Hunger, R.; Pettenkofer, C.; Scheer, R. Dipole Formation and Band Alignment at the Si(111)/CuInS₂ Heterojunction. *J. Appl. Phys.* **2002**, 91, 6560–6570.
- (58) Abrahams, S. C.; Bernstein, J. L. Piezoelectric Nonlinear Optic CuGaS₂ and CuInS₂ Crystal Structure: Sublattice Distortion in AIBIIC₂VI and AIIBIVC₂V Type Chalcopyrites. *J. Chem. Phys.* **1973**, 59, 5415–5420.
- (59) Jumpertz, E. A. Electron-Density Distribution in Zinc Blende. *Zeitschrift fuer Elektrochemie* **1955**, 59, 419–425.
- (60) Mueller, W. J.; Loeffler, G. Zur Kenntnis Der Faerbung von Gefaelltem Cadmiumsulfid. *Angew. Chemie (German Ed.)* **1933**, 46, 538–539.

- (61) Stallworth, P. E.; Guillemoles, J. F.; Flowers, J.; Vedel, J.; Greenbaum, S. G. NMR Studies of CuInS₂ and CuInSe₂ Crystals Grown by the Bridgman Method. *Solid State Commun.* **2000**, *113*, 527–532.
- (62) De Mello Donegá, C.; Hickey, S. G.; Wuister, S. F.; Vanmaekelbergh, D.; Meijerink, A. Single-Step Synthesis to Control the Photoluminescence Quantum Yield and Size Dispersion of CdSe Nanocrystals. *J. Phys. Chem. B* **2003**, *107*, 489–496.

Table of Contents Graphic

